Journal of Renewable Energy and Sustainable Development (RESD) Volume 12, Issue 2, December 2026, e-ISSN 2356-8569
http://dx.doi.org/10.21622/RESD.2026.12.2.1992

Received: 09 March 2026 Accepted: 06 July 2026 Published: 02 September 2026

A Hybrid Fast-Charging Station for Electric Vehicles Integrating Cascaded Interleaved AC–DC Converter, Renewable Energy Sources, and Battery Storage

Bader N. Alajmi [1*], Ibrahim Abdelsalam [2], and Nabil A. Ahmed [3]

[1*,3] Public Authority for Applied Education and Training, College of Technological Studies, Department of Electrical Engineering, Shuwaikh, Kuwait

[2] Arab Academy for Science, Technology & Maritime Transport (AASTMT), College of Engineering and Technology, Department of Electrical and Control, Cairo, Egypt

bn.altaweel@paaet.edu.kw, i.abdelsalam@aast.edu, na.ahmed@paaet.edu.kw

Abstract

This paper presents the design of a hybrid fast-charging station for electric vehicles (EVs). It integrates a photovoltaic (PV) generation system, a battery energy storage (BESS) system, and a two-stage non-inverting AC–DC converter within a DC bus architecture that acts as a microgrid. The proposal aims to reduce reliance on the electrical grid while ensuring stable and highly efficient performance under varying operating conditions. The PV and BESS systems are interconnected via nested DC–DC converters to improve Efficiency and minimize current stress on power components. The front AC–DC converter utilizes an inverted Buck–Boost architecture to maintain a constant DC bus voltage and draw a high power factor sinusoidal current from the grid. A single active bridge converter is employed to synchronize the DC bus voltage with the EV battery requirements. The effectiveness of the proposed control strategies was validated using PSCAD/EMTDC simulations of multiple dynamic scenarios, including sudden changes in solar irradiance and multiple charging ports. In addition, the results of the miniature experimental model confirm the system's ability to start up smoothly, achieve a high power factor, and effectively regulate voltage and current, making it suitable for modern fast charging stations.

Index-words: *EV Charging, Fast-Charging, Interleaved AC–DC Conversion, Battery Energy Storage, Renewable Energy Sources.*

I. Introduction

In recent years, the world has witnessed a significant increase in awareness of the dangers of environmental pollution, the repercussions of climate change, and global policies supporting clean energy. This has prompted many countries to gradually shift from fossil fuel-powered vehicles to electric vehicles (EVs). With governments adopting incentive programs to encourage individuals to purchase EVs, the number of EVs on the roads has increased rapidly, making it essential to develop a suitable charging infrastructure to keep pace with this accelerating demand for charging power[1].

The Society of Automotive Engineers (SAE) classifies EV charging systems into three levels [2]. Level 1 relies on a single-phase household power supply and is the least powerful in terms of electrical capacity, characterized by a low charging rate that can take up to 11 hours to complete a full charge. Level 2, prevalent in workplaces and public charging stations, uses a three-phase power supply of up to approximately 19.2 kilowatts, reducing charging time to about 4 hours. In Levels 1 and 2, the power electronics converter used for charging is part of the vehicle's drivetrain and is known as an on-board charger (OBC). Due to the need to minimize the weight and size of this component within the vehicle, its rated power is limited, which impacts charging time[3]. To overcome these limitations, the off-board charger concept emerged for Level 3 fast charging. In this level, the power converter is detached and placed outside the vehicle, while the battery is directly supplied with high-voltage DC power. This allows for charging power of up to 350 kW and operating voltages ranging from 400 V to 1000 V [4]. These high power levels enable fast charging, reaching up to 80% of the battery's capacity in 20 to 60 minutes. Due to the significantly shorter charging times

* Corresponding author

offered by fast charging technologies compared to other charging methods, these technologies have garnered increasing attention in recent years. Public fast charging stations are expected to play a pivotal role in promoting the widespread adoption of electric vehicles in the near future[5, 6].

In recent years, Level 3 fast charging stations have seen a steady increase in nominal capacity, coinciding with the significant rise in electric vehicle battery capacities. During fast charging, large and sudden amounts of power are drawn from the electrical grid, which, in the absence of coordinated charging strategies, can lead to negative impacts on the distribution network, including sharp voltage drops during charging periods, strain on distribution transformers due to increased loads, and increased power losses, especially when multiple fast charging units are operating simultaneously [7-9]. To mitigate these impacts and promote the global shift towards green transportation, the concept of hybrid charging stations has been proposed, relying on the integration of renewable energy sources (RES) as a supplementary source to meet the high-capacity charging needs of Level 3 stations [10, 11]. Solar photovoltaic (PV) power is the most widespread and suitable option in many countries, with projections indicating that between 20% and 25% of global generating capacity by 2050 will come from PV systems [12, 13]. However, integrating PV systems into fast charging stations faces significant challenges due to the fluctuating and unstable nature of solar radiation [14, 15]. To overcome this problem, the use of battery energy storage systems (BESS) is essential for improving operational Efficiency, extending component lifespan, increasing reliability, and achieving greater economic viability for fast charging stations[16-18].

The development of renewable-energy-based infrastructure and smart energy management solutions is therefore considered an important pathway toward improving energy sustainability and supporting future electrified transportation systems [19-21]. A hybrid fast charging station can be considered a DC grid, where its various components can be connected via either an AC microgrid or a DC microgrid [11]. AC microgrid connection offers a higher level of maturity in terms of protection and power metering standards compared to a DC connection. However, this configuration requires an AC-DC conversion stage followed by a DC-DC conversion stage for each individual charging port, increasing the overall cost and size of the station, as well as reducing the overall system efficiency [22]. In contrast, DC-micro grid connection requires only one AC-DC converter to connect to the electrical grid, which contributes to lower costs, reduced equipment size, and increased overall system efficiency. However, protection and metering standards for DC systems are still under development, presenting a challenge that must be considered when designing this type of charging station[23, 24].

An AC-DC converter is used to connect a fast-charging station to the electrical grid. This Converter is required to supply the charging system with the necessary continuous power to charge the electric vehicle, drawing a sinusoidal current and a high power factor, while minimizing total harmonic distortion (THD) [25]. A two-level, three-phase PWM-based rectifier is used as an AC-DC converter in electric vehicle charging applications, as mentioned in [26, 27]. However, with increasing nominal power and higher DC bus voltage, the Neutral-Point-Clamped (NPC) converter is a suitable option for fast-charging stations[28, 29], as it features lower harmonic distortion and reduced stress on switching elements compared to the two-stage rectifier [30]. The Vienna unidirectional converter has also been proposed for fast-charging applications for electric vehicles, as mentioned in [31], due to its superior technical characteristics such as high power density, high Efficiency, and very low THD [32]. A bidirectional version of the Vienna rectifier was developed to support vehicle-to-grid (V2G) operation, enabling power exchange between the vehicle and the grid [33]. Studies in [25] demonstrated the feasibility of using a conventional bridge rectifier followed by an Interleaved Boost Converter. This configuration offers the advantage of reducing current strain on power elements and increasing overall system efficiency. However, the main weaknesses of this Converter are its poor fault-blocking capabilities and the high impulse currents in the DC-side capacitors. These issues were addressed by the Interleaved Cascaded Non-Inverting buck-boost AC-DC converter proposed in[34]. Furthermore, [35] demonstrated that using a Non-Inverting Buck-Boost converter in fast charging stations provides dynamically stable performance throughout the entire charging cycle and covers a wide range of operating voltages, making it a suitable option for fast charging applications with varying voltages [35].

This paper proposes the design of a hybrid fast charging station for electric vehicles, consisting of four interconnected main units that together form a DC microgrid. The first component is a PV farm, which is connected to the DC bus via an interleaved boost converter to reduce current strain on the power electronics and improve operational Efficiency. The second component is a BESS, which is connected to the DC bus via an interleaved non-isolated bidirectional DC-DC converter. This system stores excess energy generated by the PV when production exceeds the required charging capacity and supplies power to the system when PV output falls below charging needs. The third component is an active front-end rectifier, which utilizes the interleaved non-isolated buck-boost Converter proposed in [35] due to its significant advantages, such as modular design, ease of expansion, and ability to shield DC-side faults. The primary function of this Converter is to maintain the stability of the DC bus voltage by regulating the power drawn from the electrical grid, ensuring a sinusoidal current draw and a power factor close to one. The fourth component is the electric vehicle charging ports, where a Single Active Bridge DC-DC converter is used to match the DC bus voltage with the battery pack voltage inside the electric vehicle, providing efficient charging that meets the battery's requirements. The control strategies for each component of the proposed charging station are discussed, and the overall system performance is verified under various operating conditions using PSCAD/EMTDC software. Furthermore, experimental results from a scaled-down model are presented to verify the performance of the grid interface converter and the single active bridge converter in diverse operating scenarios. To clearly highlight the novelty of the proposed work compared to existing studies, Table 1 presents a comprehensive comparison of the suggested charging station and the electric vehicle chargers discussed in the literature survey. Although Table 1 indicates that the proposed system shares several common features with previously published studies, the technical contribution of the present work extends beyond the existing literature. While Ref. [5] presents a hybrid EV charging station with an energy management strategy, its main contribution focuses on system-level energy coordination using conventional converter implementations. The design methodology, operating-mode analysis, and experimental validation of the grid-interface AC–DC converter are beyond the scope of that work. In addition, the EV charging demand is represented as a fixed electrical load without considering the practical battery charging dynamics. In contrast, the present work integrates both converter-level and system-level contributions. A complete design methodology, coordinated control strategy, and operating-mode analysis are developed for the grid-interface AC–DC converter and experimentally validated. Furthermore, the EV is modeled as a battery load operating according to the practical CC/CV charging profile, enabling realistic charging behavior. Unlike our previous studies [33] and [35], which primarily focused on individual converter topology and control, the present work investigates the coordinated operation of multiple power converters operating simultaneously under different control modes within a complete hybrid charging station. Consequently, the proposed system provides an integrated framework that combines converter design, coordinated control, realistic EV battery charging, and hybrid energy management within a unified charging station.

Table 1: A comprehensive comparison of the suggested charging station and the electric vehicle chargers discussed in the literature survey.

Feature / Aspect	[3]	[5]	[22]5	[34], [3]	Proposed Work
Focus Level	Converter	System level	Converter	Converter	System level + Converter
AC–DC Converter Design	Yes	Yes	Yes	Yes	Yes
Renewable Energy Integration (PV)	No	Yes	No	No	Yes
Battery Energy Storage (BESS)	No	Yes	No	No	Yes
DC Microgrid Architecture	No	Yes	No	No	Yes
Coordinated Multi-Source Control	No	Yes	No	No	Yes
Multi-Port EV Charging	Limited	Yes	No	No	Yes
Dynamic Scenario Analysis	Limited to a single EV	Limited (without EV battery charging mode (CC/CV))	Limited to a single EV	Limited to a single EV	Extensive
Experimental Validation	NO	NO	NO	YES	System-level

http://dx.doi.org/10.21622/RESD.2026.12.2.1992

II. The proposed hybrid charging station

The proposed hybrid charging station is illustrated in Figure 1. It comprises four primary components, which are interconnected via a DC-bus to establish a micro-DC grid. The first component is the renewable energy sources; in this paper, PV technology is employed, and a two-phase interleaved converter is utilized to transfer the harvested PV energy to the micro-DC grid, thereby distributing the current load across the power electronic devices. The second component is the battery energy storage system (BESS), which is utilized to store excess PV energy when the available PV output exceeds the required power for EV charging. This stored energy will be utilized when the demand for EV charging power surpasses the available PV output. An interleaved bidirectional DC-DC converter is implemented to connect the BESS to the micro-DC grid busbar. The third component is a three-phase non-inverted AC-DC converter, which supplies DC power from the utility grid when necessary. For instance, if the combined output from the PV and BESS is inadequate for EV charging, the remaining power will be sourced from the utility grid. Additionally, this Converter can be used to charge EVs overnight or to recharge the BESS during off-peak hours at lower tariffs. The fourth component consists of EV fast charging sockets; for simplicity, a single active bridge (SAB) DC-DC converter is employed to align the DC-bus voltage with the EV battery bank.

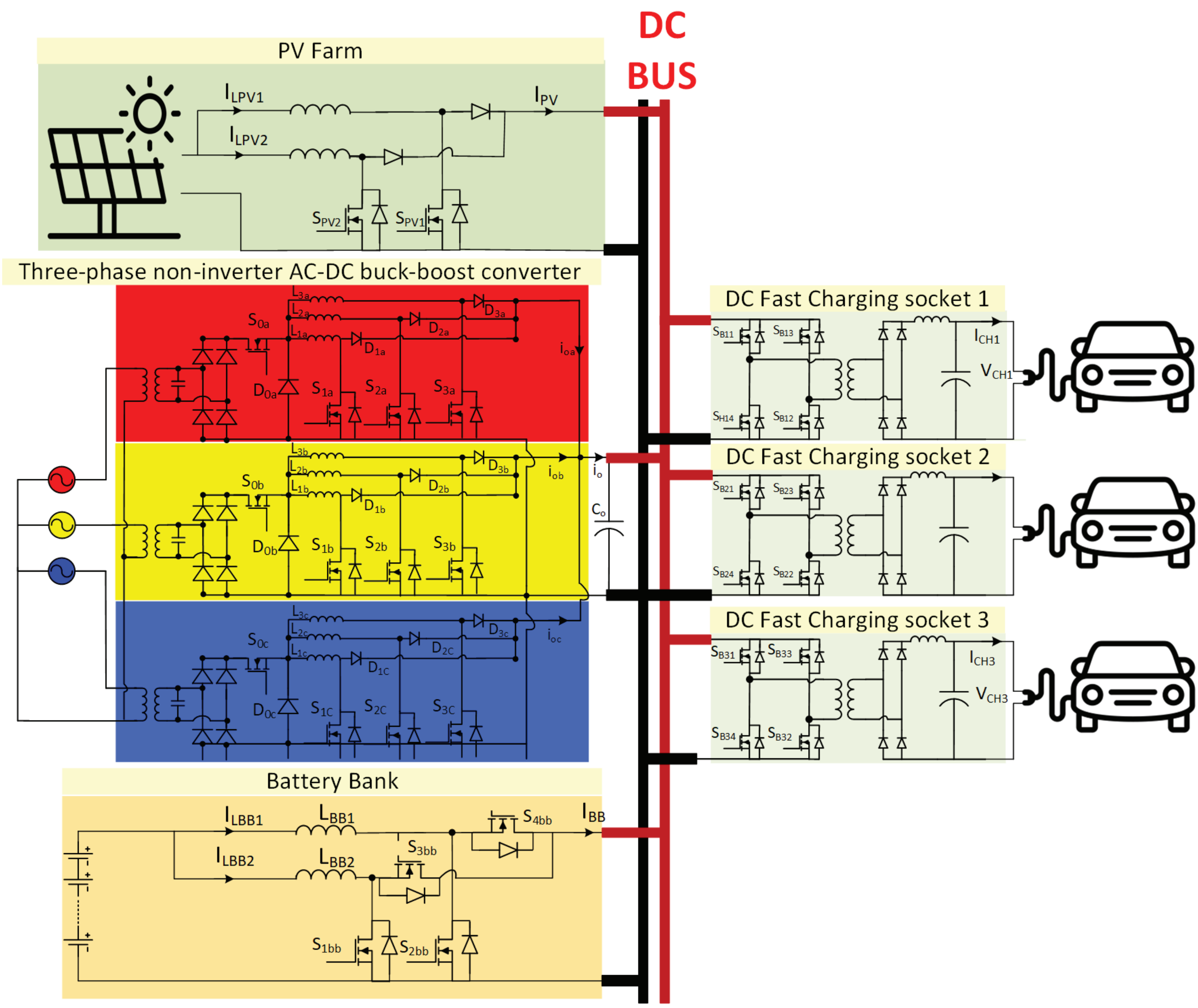

Figure 1: proposed a hybrid charging station.

Volume 12, Issue 2, December 2026, e-ISSN 2356-8569
http://dx.doi.org/10.21622/RESD.2026.12.2.1992

Figure 1 clearly illustrates that the proposed charging station is designed to be scalable and incorporates a modular design. Under optimal conditions involving renewable energy resources, BESS, and an AC-DC converter, this hybrid charging station has the potential to significantly lessen the strain on the utility grid.

III. Cascaded non-inverter AC-DC converter

Figure 2 shows a single module of the proposed AC-DC converter, which consists of two cascaded stages. The initial stage is a buck converter that is positioned after a bridge rectifier, while the subsequent stage is made up of a three-phase interleaved boost converter. The gating sequence for the cascaded non-inverting ac-dc Converter is illustrated in Figure 3. For instance, the interleaved boost converter switches (S1, S2, and S3) receive gate signals that are shifted by 120 degrees, and the buck switch (S_0) is activated when any of the interleaved boost converter switches are turned on to allow current to flow from the supply to charge the interleaved converter switches. In case of the high voltage gain required, and if the duty cycle exceeds 1/3, the buck switch will remain continuously on, causing the proposed Converter to function similarly to a conventional interleaved boost converter. The integration of these two stages offers numerous advantages, such as a single-stage buck-boost capability with a seamless transition from buck mode to boost mode, a soft startup feature, and the capacity for the buck switch to limit or stop the fault current in the case of a load fault.

In the proposed cascaded non-inverting AC–DC converter, a phase-shifted interleaving technique is adopted to reduce the DC-link voltage ripple and capacitor current stress. Within each converter module, the three interleaved branches are operated with a phase shift of 120° between their switching signals. This phase displacement increases the effective ripple frequency observed at the DC side and provides partial cancellation of the high-frequency current components. Moreover, an additional phase shift is introduced between the three converter modules connected to the different phases, which further increases the equivalent ripple frequency of the DC-link capacitor charging current. As a result, the DC-link capacitor receives a higher-frequency and more continuous charging current, leading to a significant reduction in the output voltage ripple and the required DC-link filtering requirements.

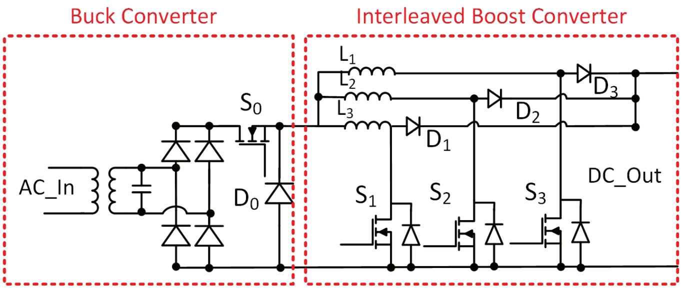

Figure 2: Cascaded non-inverter AC-DC buck-boost module.

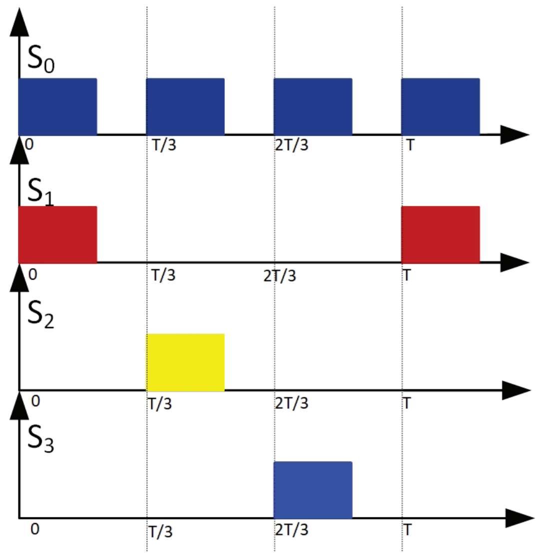

Figure 3: Cascaded non-inverting AC-DC converter gating sequence.

The operation of discontinuous current mode (DCM) is essential for maintaining sinusoidal waveforms of the supply current. To achieve DCM operation, the inductances of the interleaved ac-dc converter must be designed to values that are below the critical threshold Lc.

The peak current of any interleaved inductor is calculated from:

$$I_1 = k_{ac-dc}\, V_p \sin \omega t_s / fL \tag{1}$$

where $k_{ac\text{-}dc}$ is the duty ratio of the ac-dc interleaved converter, V_p is the peak ac voltage, ω is the angular frequency of the supply voltage, t_s is the switching instant, V_{dc} is the dc bus voltage, f is the switching frequency, *and* L is the inductance of any interleaved coil. The fall time of the inductor current is expressed as

$$\lambda = \frac{L\, I_1}{V_{dc} - V_p \sin \omega t_s} \tag{2}$$

Using (1) and (2), the average current fed to the DC bus is estimated as follows:

$$I_{dc} = \frac{3k_{ac-dc}}{2fL}\int_0^{\pi}\frac{V_p^2\sin^2\omega t_s}{V_{dc}-V_p\sin\omega t_s}d\omega t_s = P_o/3V_{dc} \quad (3)$$

The output power from the interleaved AC-DC converter can be estimated from:

$$P_o = \frac{9k_{ac-dc}^2V_{dc}^2}{2\pi fL}\left[\frac{2g}{\sqrt{g^2-1}}\left(\frac{\pi}{2}+tan^{-1}\frac{1}{\sqrt{g^2-1}}\right)-\frac{2}{g}-\pi\right] \quad (4)$$

where $g=V_{dc}/V_p$. At $\omega t_s = \pi$, the maximum fall time of the inductor can be estimated using (1) and (2) as

$$\lambda = \frac{k_{ac-dc}}{f(g-1)} \quad (5)$$

The boundary condition between the discontinuous current mode and continuous current mode can be estimated from (5) as follows:

$$g_{BC} = \frac{1}{1-k_{ac-dc}} \quad (6)$$

To express the critical inductance, substitute (5) and (6) in (4) and rearrange it as follows:

$$L_{cr} = \frac{9k_{ac-dc}^2V_{dc}^2}{2\pi fP_o}\left[\frac{2g_{BC}}{\sqrt{g_{BC}^2-1}}\left(\frac{\pi}{2}+\tan^{-1}\frac{1}{\sqrt{g_{BC}^2-1}}\right)-\frac{2}{g_{BC}}-\pi\right] \quad (7)$$

It is important to highlight that configuring the inductors of the interleaved AC-DC converter at L_c guarantees the operation at boundary conditions during peak supply voltage instances.

The current rating of the switches used for the interleaved DC-DC converters used for the battery pack and PV module can be calculated from:

$$I_p = \frac{k_{dc-dc}\,V_i}{L_{dc-dc}\,f_s} \quad (8)$$

where k_{dc-dc} is the duty ratio of the dc-dc interleaved converter, V_i is the input dc voltage, f_s is the switching frequency, and L_{dc-dc} is the inductance of each interleaved coil.

IV. Control scheme

The proposed control scheme has two primary requirements. The first requirement is to minimize reliance on the utility grid, ensuring that the majority of the charging power is sourced from renewable energy resources and the BESS. The second requirement is to guarantee that each power electronics converter operates smoothly under varying load dynamic conditions. The proposed hybrid charging station consists of four main control loops: 1- AC-DC converter control loop, 2- converter control loop, 3- battery bank control loop, and 4- SAB control loop.

A. AC-DC converter control loop

The primary function of the AC-DC converter controller is to maintain a stable DC-Bus voltage while producing a sinusoidal current at nearly unity power factor from the grid. In this manuscript, the DC-Bus is configured to 800V. If the DC-Bus voltage surpasses 800V, the AC-DC converter will promptly reduce the power received from the grid. Conversely, if the DC-Bus voltage decreases, the AC-DC converter will increase the power received from the grid. Figure 4 illustrates the proposed control scheme designed to meet this requirement. The control of the AC-DC converter comprises three main cascade control loops. The first loop is the DC-Bus voltage control loop, where the error between the reference voltage and the actual DC-Bus voltage is processed through a proportional integral (PI) controller to derive the converter DC-output reference current (I_{o_ref}). As depicted in Figure 4, a current limiter is implemented to restrict the Converter's DC output current, thereby preventing overload of the proposed Converter. In the event of a load failure, this current limiter will activate to limit the fault current. The second loop takes the reference DC output current and employs another PI controller to determine the reference grid AC current. An additional current limiter is utilized to ensure that the Converter does not receive more than its rated input power. The reference grid AC current is then fed into three power factor correction loops, one for each phase, as clarified in Figure 4. The power factor correction control loops first synchronize the reference grid AC current by multiplying it with the corresponding absolute unity value of the respective phase voltage, as shown in Figure 4. The error between the synchronized absolute grid AC current and

http://dx.doi.org/10.21622/RESD.2026.12.2.1992

the absolute value of the grid current is processed through a PI controller to obtain the modulation index for the corresponding cascaded non-inverter AC-DC converter module. This modulation index is then compared with three carriers shifted by 120 degrees to generate the gate signal for the interleaved boost converter. For the buck switch gate signal, an OR logic gate is employed, as illustrated in Figure 4.

B. PV converter control scheme

Figure 5 illustrates the control loop of the PV converter, which receives the reference PV current (I_{PV_ref}) derived from various maximum power point tracking techniques; in this paper, the perturb and observe method was employed for simplicity. Subsequently, a PI controller estimates the V_{dc_ref} based on the discrepancy between the reference PV current and the actual PV current. A voltage limiter is essential for the safety of the Converter and all other components connected in parallel, particularly in scenarios where the battery bank is fully charged, no electric vehicles (EVs) are connected, or the charging power is less than the available PV power. Without this voltage limiter, the PV converter would continue to increase the DC-bus voltage, which could adversely affect the safety of other devices. In such cases, the voltage limit will cease tracking the maximum point and will only supply the necessary power for the current situation. The second loop consists of voltage control loops, where a PI controller is utilized to determine the modulation index for the interleaved boost converter.

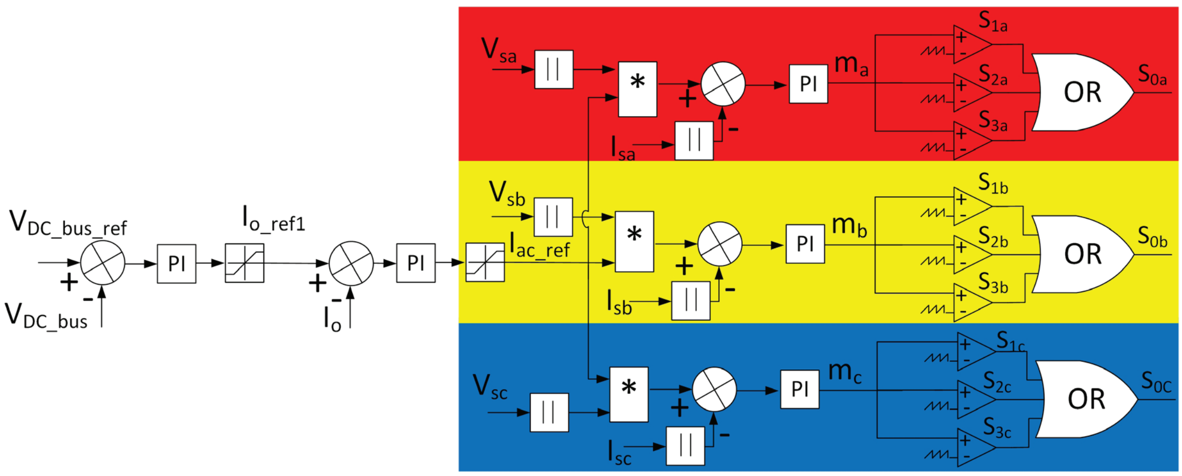

Figure 4: proposed the AC-DC converter control loop.

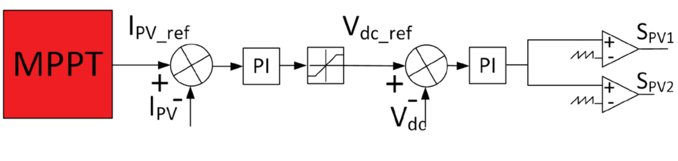

Figure 5: PV converter control loop.

C. Battery bank control scheme

The BESS is integrated into the system to reduce the operational costs of the entire charging station, as it charges when the available PV power exceeds the required EV charging power, or during periods of low-cost off-peak electricity tariffs.

The initial function of the BESS is to ascertain the reference battery current and to determine whether the battery bank is in a charging or discharging state. The reference battery bank current (I_{BB_ref}) is computed by dividing the difference between the total EV charging power and the total PV power supplied to the DC-bus by the battery bank voltage, as clarified in Figure 6. If I_{BB_ref} is positive, this indicates that the battery bank will function in discharging mode, with the corresponding active switches being S_{1BB} and S_{2BB}. Conversely, if the value is negative, it signifies that the battery bank will operate in charging mode, activating switches S_{3BB} and S_{4BB}, as shown in Figure 1.

A PI controller will be employed to estimate the modulation index of the BESS converter based on the error between I_{BB_ref} and the actual battery bank current (IBB).

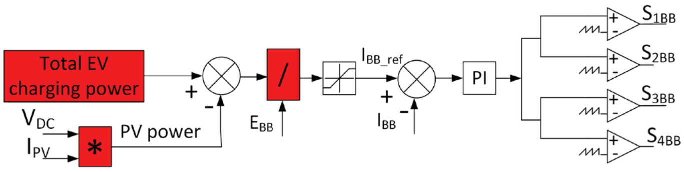

Figure 6: Battery bank control loop.

D. SAB controller

The SAB controller is required to match the DC bus voltage with the voltage of the EV battery bank, while also overseeing the charging process to ensure a smooth transition between voltage control mode (VCM) and current control mode (CCM). For the operation of the modular, each EV charging socket is equipped with its own control loop. Figure 7 illustrates the control scheme for a single EV charging socket, which comprises two primary loops: the outer controller and the inner controller. The outer controller is responsible for VCM; it receives the reference battery voltage from the EV battery management system and, based on the battery voltage error, estimates the reference battery charging current using a PI controller. In the inner control loop, the phase shift for the SAB is calculated from the error in the battery charging current, as depicted in Figure 8.

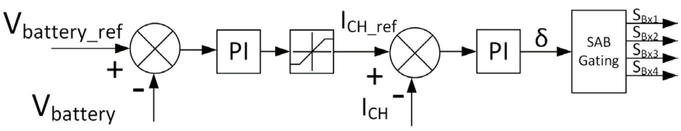

Figure 7: SAB control loop.

V. Simulation results

The effectiveness of the proposed charging station has been evaluated and confirmed with PSCAD/EMTDC software. The specifications of the system are outlined in TABLE 2. To evaluate the dynamic performance and ensure that every component of the charging station adheres to the rule-based operation in coordination with the others, the operational scenario includes seven cases. The key waveforms that summarize the performance of the proposed charging station are shown in Figures 8 to 16. It should be noted that the full rated power of the grid-interface converter represents its maximum available capability rather than its normal operating condition. Under the proposed energy management strategy, the photovoltaic array and the battery energy storage system supply most of the EV charging demand, while the grid-interface converter compensates only the required power deficit. Consequently, during normal operating conditions, each converter module typically operates at approximately 30% of its rated power. Therefore, the converter inductance was designed based on this practical operating region rather than the maximum converter rating. During high loading conditions, the Converter naturally transitions from DCM to CCM, while the proposed PFC control loop maintains sinusoidal grid current, low THD, and near-unity power factor over the entire operating range.

Table 2: Simulation setup parameters.

PV farm parameter at 25°at 1000W/m²	
Rated power	60kW
Open circuit voltage	748V
Short circuit current	117.6A
Voltage at Maximum Power	622.5V
Current at Maximum power	97A
Interleaved converter switching frequency	50kHz
Interleaved converter inductance	500uH
AC-DC convert parameter	
Rated power	180kW
Switching frequency	20kHz
Single-phase AC-side transformer rated power	60kW
Single-phase AC-side transformer rated voltage ratio	220/220
dc-side inductance	500uH
dc-side capacitance	2200uF
Battery energy storage system	
Rated power	60kW
Battery bank voltage	600V
Switching frequency	50kHz
Converter inductance	500uH
Single active converter parameters	
Switching frequency	25kHz
Transformer ration	800/550V
Maximum charging current	100A
Output L-C filter	100uH, 100uF

A. Case '1'

In case '1' initiates, the AC-DC converter begins to build up the DC bus voltage as illustrated in Figure 8. And the solar irradiance was set to 1000W/m². During this case, all the PV power is transferred to the BESS.

B. Case '2'

Case '2' starts once the DC voltage surpasses 750V, the PV MPPT converter becomes active, and simultaneously, the BESS commences operation in changing mode. During case '2,' the DC bus is built and reaches its steady-state value of 800V as shown in Figure 8. The results depicted in Figure 9 indicate that all PV power is being stored in the BESS. Furthermore, Figure 10 demonstrates that the PV converter successfully tracks the reference current with satisfactory performance. Figure 11 illustrates the BESS current, clearly showing that the implemented controller effectively tracks the reference current. According to the rule-based operation, the current is negative, as all PV power is being transferred to the BESS.

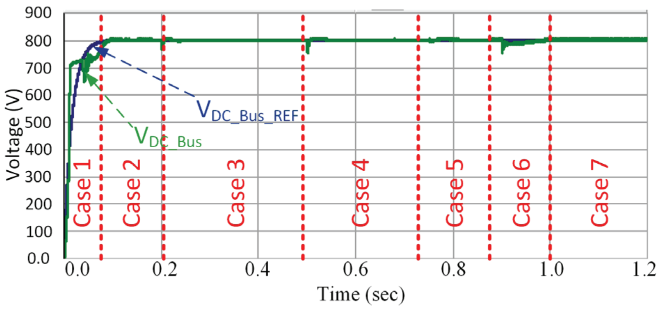

Figure 8: DC Bus voltage.

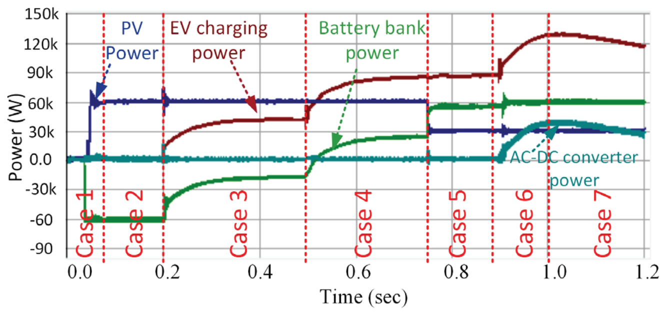

Figure 9: PV power, battery bank power, AC-DC converter power, and total charging power.

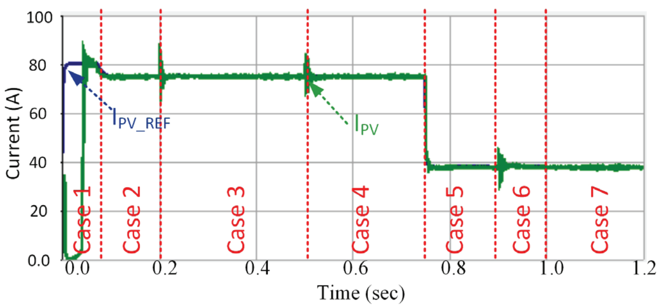

Figure 10: MPPT reference PV current and PV current.

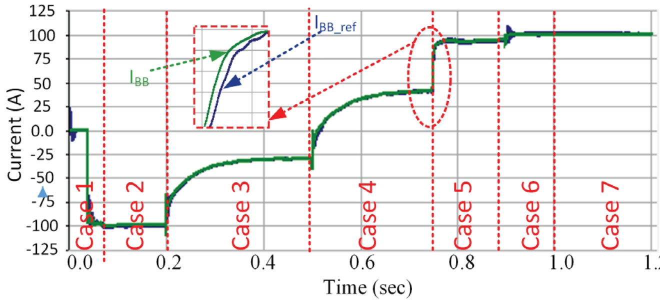

Figure 11: Battery bank current.

C. Case '3'

In case '3,' the First EV charging socket is connected to a 400V EV battery bank, and the charging process commences at CC (with a rated current of 100A). This can be seen in Figure 12. Additionally, Figure 12 illustrates that the voltage of the EV battery begins to rise as a result of the charging process. In case '3', the power for EV charging is sourced from the PV farm. Figure 12 indicates that during case '3', the PV power remains constant due to the absence of changes in solar irradiance. However, the charging power for the BESS will experience a gradual reduction, as a portion of the available PV power is allocated to EV charging. The decline in the reference BESS current can be observed in Figure 11 during case '3' to offset the reduction in the available charging power for the BESS.

D. Case '4'

The second EV charging socket is activated in case '4', as depicted in Figure 13. At the onset of case '4', the charging power of the BESS begins to decrease as the second charging socket's power intake rises, leading to a situation where the total charging power demand surpasses the available PV power. In accordance with the rule-based operation, the BESS will operate in discharging compensate for the required necessary charging power, as outlined in Figure 9 and Figure 11 during case '4'.

http://dx.doi.org/10.21622/RESD.2026.12.2.1992

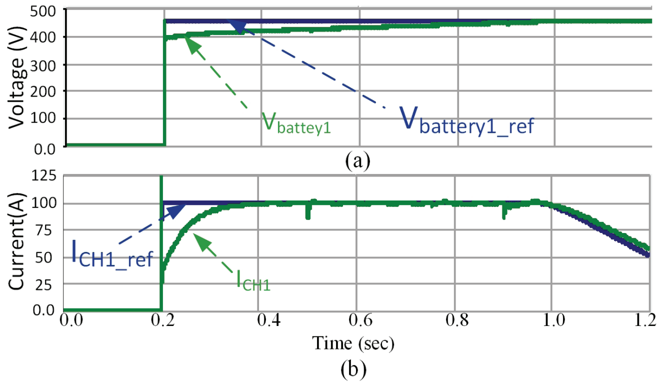

Figure 12: EV charging socket 1 results (a) EV battery, and (b) Charging current.

E. Case '5'

In case '5', the solar irradiance decreased to 500W/m², resulting in a reduction of the total available PV power from 60kW to 30kW. The BESS will discharge at its rated power of 60kW to compensate for the decrease in available PV power. The results illustrated in Figures 9 through 11 demonstrate the rapid response of the BESS to sudden changes within the system, highlighting the overall effective dynamic performance of the proposed charging station.

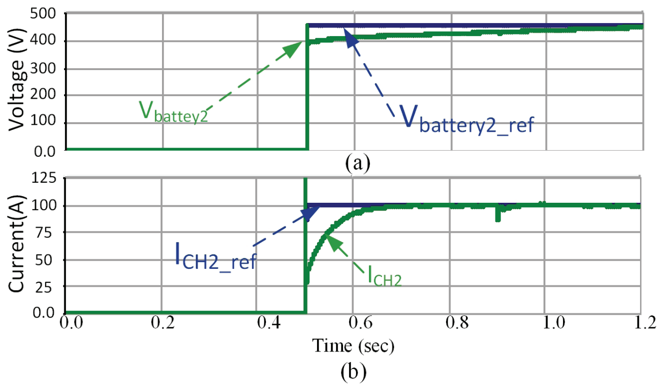

Figure 13: Charging socket 2 results. (a) EV battery reference voltage and voltage, (b) EV reference charging current and EV charging current.

F. Case '6'

The third charging socket is activated as illustrated in Figure 14. During case '6', as the total EV charging power increases, it will surpass the available PV power pulse along with the BESS rating discharging power, which tends to cause a drop in the DC bus voltage. As depicted in Figure 8, during case '6', the DC bus voltage experiences a slight decrease from its reference value. At this point, the AC-DC converter will initiate actions to maintain the DC bus at its rated value by compensating for the shortfall in the power necessary for EV charging. The results presented in Figure 9 indicate that the AC-DC converter began to supply power during case '6'. Furthermore, the results in Figure 15 illustrate the three-phase supply current and phase ' a ' voltage on the AC input side of the AC-DC converter. It can be observed that the proposed cascaded non-inverted AC-DC converter demonstrates a smooth startup with a sinusoidal supply current at nearly unity power factor.

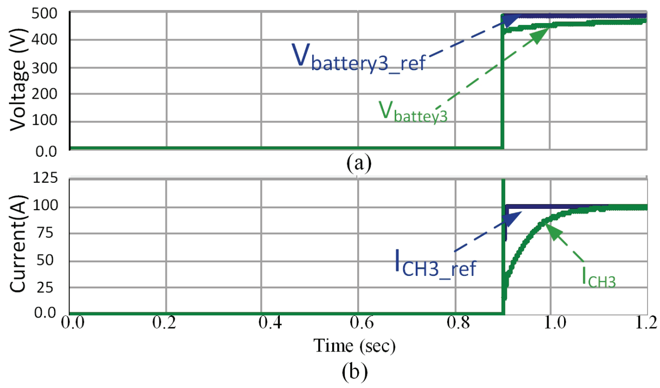

Figure 14: Charging socket 3 results. (a) EV battery reference voltage and voltage, (b) EV reference charging current and EV charging current.

G. Case '7'

In case '7', the voltage of the first charging socket connected to the EV reached its reference value, prompting the charger controller to switch from CC mode to CV mode, as depicted in Figure 12'a' and 'b'. As shown in Figure 12, the charging current is falling, which tends to decrease the overall required charging power. According to the rule-based operation, the power delivered by the AC-DC converter will decrease to lessen the reliance on the AC grid power. The results presented in Figure 9 indicate a reduction in the total required EV charging power and a decrease in the charging power of the AC-DC converter, while the PV power and BESS remain constant throughout case '7'. Figure 16 illustrates that the grid-derived current experiences a reduction due to the decrease in the required power delivered by the AC-DC converter.

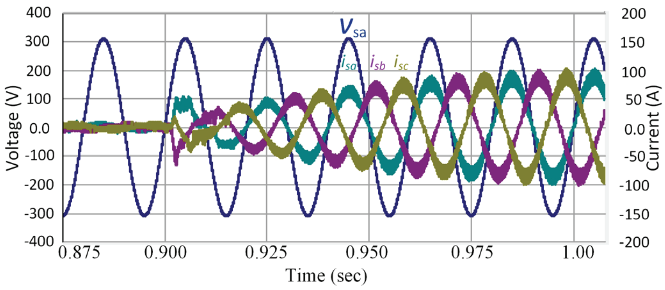

Figure 15: three-phase supply current and phase ‘ a ‘ voltage at the beginning of case ‘6’.

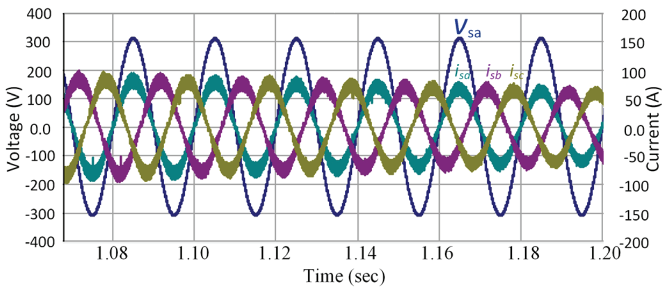

Figure 16: three-phase supply current and phase ‘ a ‘ voltage during case ‘7’.

The Efficiency of the proposed system was evaluated using the steady-state power values extracted from Figure 9 for each operating condition and summarized in Table 3. It should be noted that the power curves in Figure 9 were obtained through dynamic simulation using PSCAD/EMTDC software, where the system undergoes several different operating conditions. To ensure the accuracy of the efficiency calculation, power values were taken at the end of each operating condition after the system reached steady-state mode, ensuring that all transients had dissipated and the control system operated in a stable state. Therefore, each condition represents an independent operating point, and the power values are updated and recalculated for each condition separately. The effective output power was defined as the sum of the electric vehicle charging power and the battery energy storage system (BESS) charging power in the battery charging conditions. The results show that the proposed system maintains high Efficiency across various operating conditions, ranging from 94.1% to 97.8%, depending on the number of active conversion stages and the power flow paths within the system. It was also noted that the highest Efficiency is achieved when power is transferred directly from the solar energy system to the load or to the storage system, while Efficiency decreases slightly when the number of conversion stages increases, such as in cases of battery discharge or grid support.

Table 3: System Efficiency Based on Figure. 9 operating Cases.

Case	Power Source	Total Input Power (kW)	EV Charging Power (kW)	BESS Charging Power (kW)	Estimated Efficiency (%)
Case 1	PV	60	0	58.68	97.8
Case 2	PV	60	0	58.68	97.8
Case 3	PV	60	39.2	18.6	96.3
Case 4	PV+BESS	84.4	80	0	94.8
Case 5	PV+BESS	85	80	0	94.1
Case 6	Grid+ PV+BESS	131	125	0	95.44
Case 7	Grid+ PV+BESS	121	118	0	97.5

VI. Experimental results

A simplified, miniaturized prototype was built to verify the performance of the proposed AC–DC converter integrated with an SAB under various operating conditions, such as voltage and current control modes, as well as to evaluate the AC–DC controller’s ability to regulate the DC-bus voltage. Figure 17 illustrates the experimental setup of the prototype, while the system parameters are shown in Table 4. In these experiments, the DC-bus reference voltage was set at 200 V, the SAB output voltage at 95 V, and the maximum output current was set at 7.5 A.

The results shown in Figures 18 and 19 highlight the performance of the complete system during the startup phase. Figure 18 demonstrates the synchronization mechanism between the AC–DC converter and the SAB. Upon receiving the startup signal, the AC-DC converter begins to ramp up its output voltage. When the voltage reaches 95% of

Volume 12, Issue 2, December 2026, e-ISSN 2356-8569
http://dx.doi.org/10.21622/RESD.2026.12.2.1992

its rated value, the SAB automatically activates and begins to ramp up the voltage to the reference value. CH3 represents the DC-bus voltage, while CH4 indicates the charging port voltage. Figure 19 shows the Phase ‘ a ‘ voltage and the three-phase supply current drawn from the grid during the startup phase and up to steady state, demonstrating the proposed Converter's success in drawing a high power factor sine wave current throughout operation. The results in Figures 18 and 19 show that the proposed charging station possesses stable and smooth soft-start capability, maintaining a high-quality sine wave current with a power factor close to one.

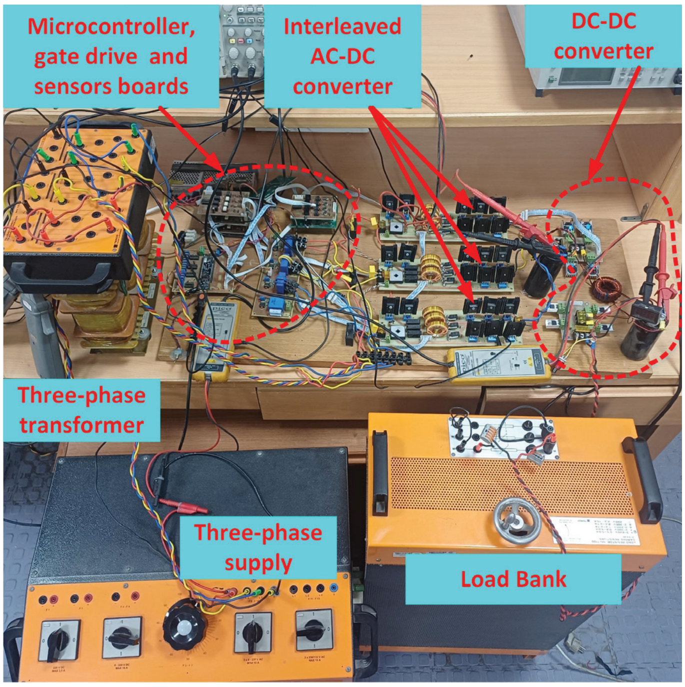

Figure 17: Experimental prototype.

Table 4: Experimental setup parameters.

AC-DC converter parameters	
Grid voltage	120V phase voltage
Rated power	1kW
Switching frequency	20kHz
Ac-side transformer	1-phase 110/66V 0.35kW
Ac-side C filters	1uf
dc-side indicates	500uH
dc-side C filter	2200uF
SAB parameter	
Rated power	600W
Switching frequency	20kHz
High-frequency transformer turns ratio	2:1
Output capacitor	1000uf

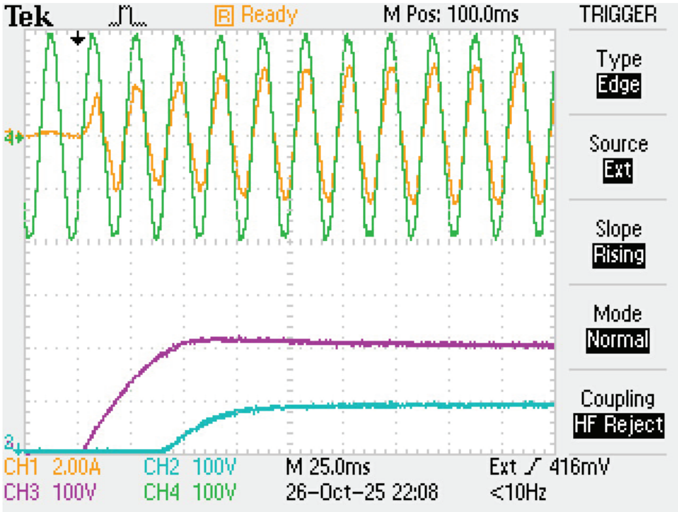

Figure 18: Performance during starting up CH1 phase ‘a’ Supply current, CH2 phase ‘a’ Supply voltage, CH3 DC-bus voltage, CH4 charging socket output voltage.

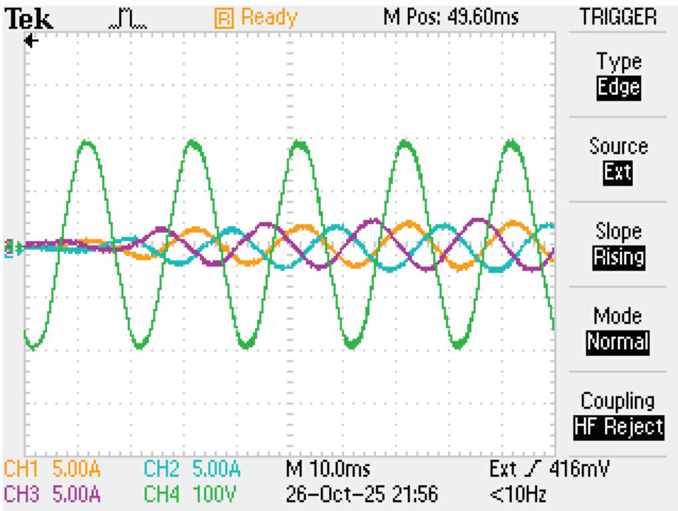

Figure 19: Phase ‘a ‘ supply voltage, and three-phase supply current during startup.

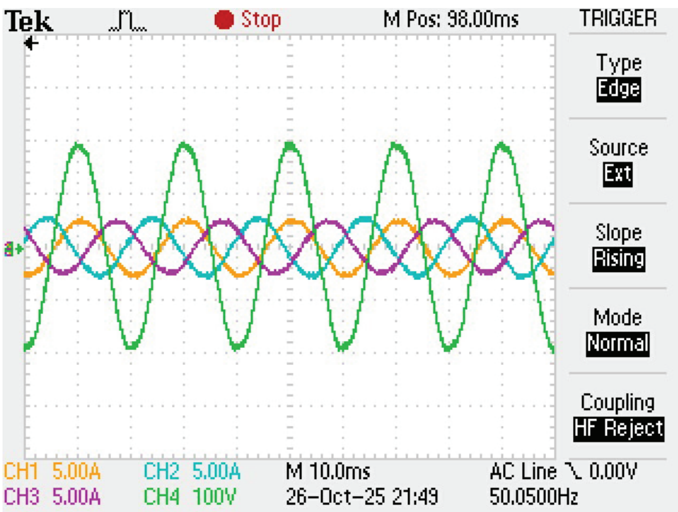

Figure 20: Phase ‘a ‘ supply voltage, and three-phase supply current during the steady state.

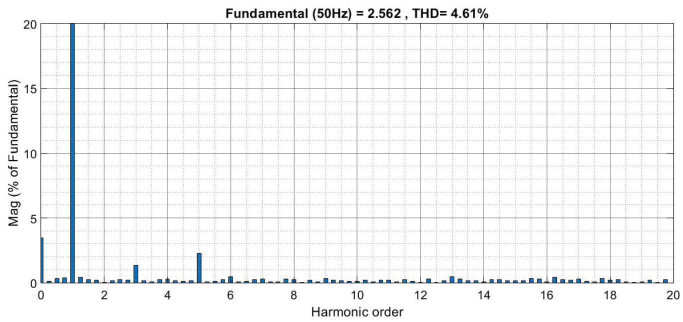

Figure 21: MATLAB Fast Fourier Transform (FFT) of phase ' a ' supply current, at steady state.

Figure 22 shows the system performance at steady state and after a sudden load change. CH1 displays the DC-bus voltage, demonstrating that the AC-DC converter successfully maintained the reference voltage even under increased load. CH2 and CH3 show the load current and voltage, respectively, and it is observed that when the resistance was reduced, the current control mode was immediately activated to maintain the current at its set value.

To illustrate the DCM operation of the proposed AC–DC converter and to validate the inductance design, the currents of a single-module interleaved inductor are presented in Figures 23 and 24. Based on Eq. (7) and considering a rated power of 1 kW for a single-phase module, the critical inductance is calculated to be approximately 540 μH. The inductance used in the experimental prototype is 500 μH. It should be noted that, due to laboratory limitations related to the available three-phase transformer rating, the maximum loading of a single module during experimental testing was limited to approximately 350 W. The results in Figure 23 show the interleaved inductor currents along with the DC-link capacitor charging current. It is evident that the inductor currents exhibit discontinuous behavior, confirming DCM operation. Additionally, it can be observed that although the inductor currents are discontinuous, the net DC-link capacitor current remains continuous. This characteristic contributes to reducing the stress on the DC-side capacitor and minimizing the output voltage ripple. Figure 24 presents the inductor currents of a single converter module operating at a 1 kW load with a DC output voltage of 200 V. The results indicate that the Converter operates near the boundary between continuous conduction mode (CCM) and discontinuous conduction mode (DCM), depending on the operating conditions.

These results collectively confirm that the proposed fast-charging architecture possesses high dynamic stability, effective voltage and current regulation capabilities, and operational Efficiency, making it suitable for practical applications in electric vehicle fast-charging stations.

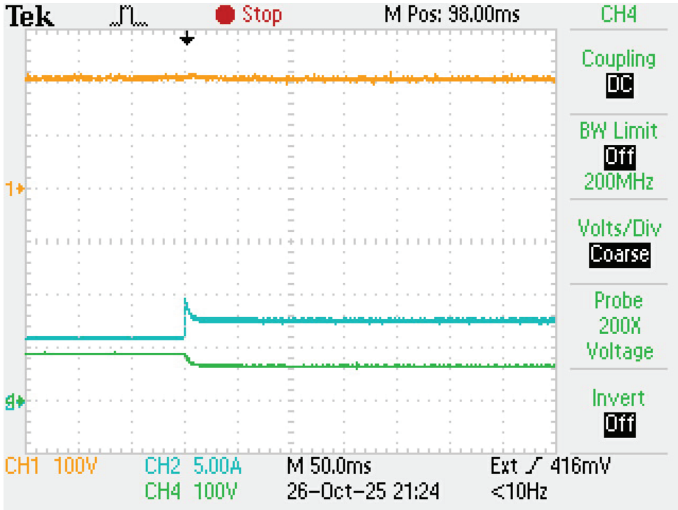

Figure 22: Proposed charger performance CH1 DC-bus voltage, CH2 and CH3 show the load current and voltage.

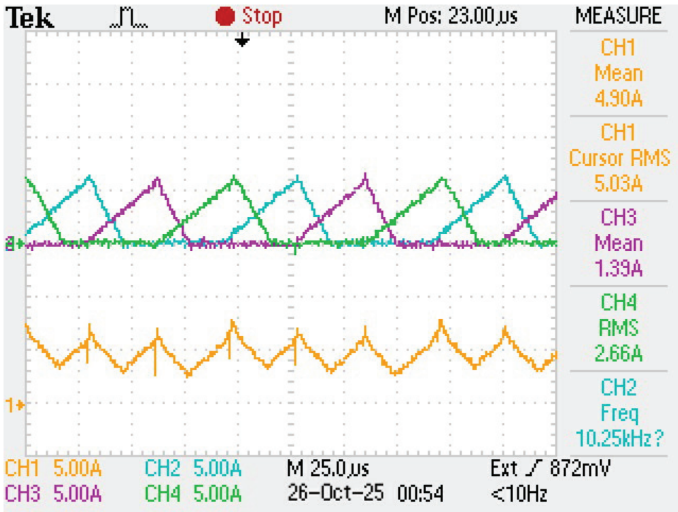

Figure 23: CH1: DC-link capacitor current; CH2, CH3, and CH4: single-module interleaved inductor currents.

Figure 25 shows the experimental DC-link capacitor charging current together with the output currents of the three-phase converter modules. The captured waveform corresponds to the operating instant around the zero-crossing region of phase-A voltage. At this instant, the voltage of phase A is almost zero; therefore, the charging current contribution from the phase-A converter module becomes approximately zero. However, due to the phase-shifted operation between the different converter modules, the remaining phases continue to supply charging current to the DC-link capacitor. It can be observed that although the output current of each individual converter module is discontinuous, the phase displacement between the modules results in a nearly continuous DC-link capacitor charging current. This confirms the effectiveness of the proposed interleaved phase-shifted operation in increasing the equivalent ripple frequency, reducing the capacitor current ripple components, and consequently minimizing the DC-link voltage ripple.

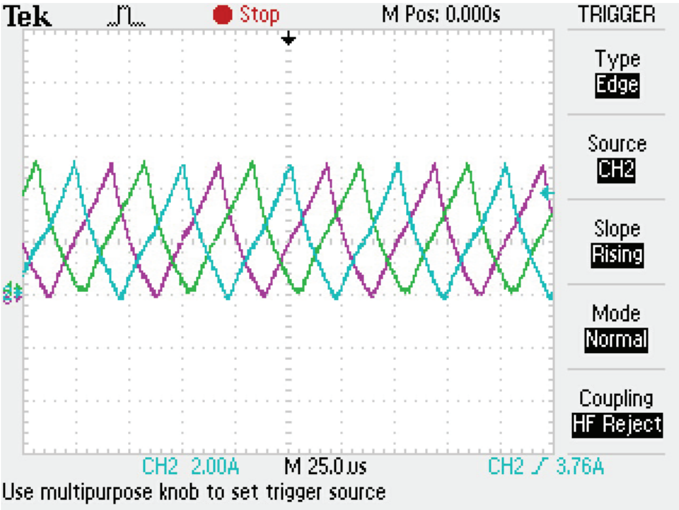

Figure 24: Single-module interleaved inductor currents when the single module operates alone at 1kW output power.

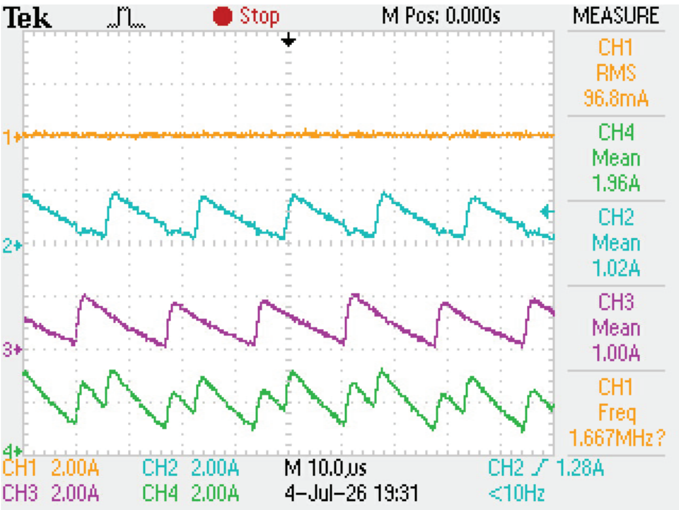

Figure 25: Shows the DC-link capacitor charging current and the three-phase module output currents around the phase-A voltage zero-crossing region (CH1-CH3: phase-module output currents; CH4: DC-link capacitor charging current).

The experimental efficiency analysis of the proposed cascaded conversion system is presented in Table 5. Figure 26 illustrates the experimental measurements used for the efficiency calculation at 372 W output power. The AC–DC converter output power, which represents the input power of the DC–DC stage, is calculated from the measured DC-link voltage and the average DC-link current delivered to the DC–DC converter. Since the DC-link voltage is regulated at 200 V, the mean value of the DC-link current is extracted from the oscilloscope measurement and multiplied by the DC-link voltage to determine the DC-DC converter output power. The DC-DC converter output power is calculated from the charging socket voltage and current measurements. The experimental results show that the AC–DC converter achieves an efficiency higher than 94.5% over the tested operating range, while the DC–DC converter efficiency varies between 95.1% and 97.5%. The slight efficiency reduction compared with the simulation results is mainly attributed to practical non-ideal effects that are not fully considered in the simulation model, including the winding resistance of the magnetic components, semiconductor parasitic losses, and transformer core losses. Moreover, the implemented DC–DC converter uses a conventional single-phase-shift (SPS) control technique; therefore, additional circulating current losses may occur at certain loading conditions. Further efficiency improvement can be achieved by adopting advanced modulation techniques, such as dual-phase-shift (DPS) or triple-phase-shift (TPS) control strategies, which can reduce circulating current and optimize converter operation over a wider load range.

Table 5: Experimental setup efficiency calculation.

AC-DC converter input power	AC-DC converter output power	DC-DC converter output power	AC-DC converter efficiency	DC-DC converter efficiency	Full system efficiency
291W	278W	271W	95.5%	97.5%	93.1%
407W	388W	372W	95.3%	95.9%	91.4%
511W	486W	465W	95.2%	95.7%	91.1%
633W	601W	573W	94.9%	95.5%	90.6%
864W	818W	779W	94.7%	95.2%	90.2%
944W	893W	849W	94.6%	95.1%	89.9%

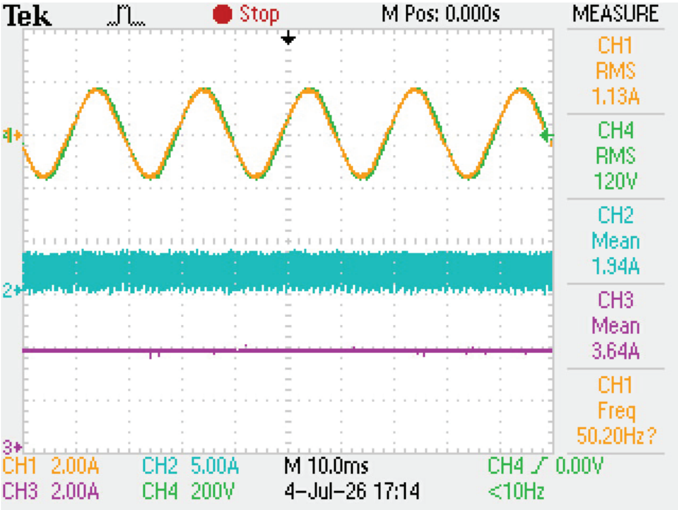

Figure 26: Performance at 372W output power CH1 phase 'a' Supply current, CH2 DC-side capacitor delivery current to the dc-dc converter, CH3 DC-DC converter output current, CH4 phase 'a' supply voltage.

VII. Conclusion

This paper presented a hybrid fast-charging station for electric vehicles based on a DC microgrid architecture integrating PV generation, BESS, and a cascaded interleaved AC–DC converter. The proposed system aims to reduce dependency on the utility grid while maintaining high Efficiency and stable operation under different operating conditions. The system performance was evaluated under seven dynamic operating cases using PSCAD/EMTDC simulations. The results demonstrated that the proposed coordinated control strategy effectively manages the power flow between the PV system, BESS, grid interface, and EV charger while maintaining a stable DC-bus voltage and reliable charging operation. The estimated system efficiency under different steady-state operating conditions ranges between 94.1% and 97.8%, depending on the number of active conversion stages and power flow paths. Furthermore, experimental validation using a scaled-down prototype confirmed the effectiveness of the proposed converter design and control strategy. The measured results show that the AC–DC converter achieves a maximum efficiency of 95.5%, while the DC–DC converter reaches 97.5%. The experimental results also verify smooth startup operation, stable voltage regulation, and high-quality input current. In addition, the adopted interleaved phase-shifted operation improves the DC-link voltage quality by increasing the equivalent ripple frequency of the capacitor charging current and reducing the DC-side ripple components. Overall, the simulation and experimental results confirm the feasibility of the proposed hybrid charging station and its capability to provide efficient and reliable operation under different charging and energy management scenarios.

Acknowledgments

The authors wish to acknowledge the public authority for applied education and training (PAAET) for providing financial support to this research (Project No. TS-23-08).

References

[1] H. A. Gabbar, Y. Elsayed, A. B. Siddique, A. Elshora, and A. Adeleke, "Design of Fast Charging Station with Energy Management for eBuses," *Vehicles*, vol. 3, no. 4, pp. 807–820, Nov. 2021, doi: 10.3390/vehicles3040048.

[2] S. Negarestani, M. Fotuhi-Firuzabad, M. Rastegar, and A. Rajabi-Ghahnavieh, "Optimal Sizing of Storage System in a Fast Charging Station for Plug-in Hybrid Electric Vehicles," *IEEE Transactions on Transportation Electrification*, vol. 2, no. 4, pp. 443–453, Dec. 2016, doi: 10.1109/tte.2016.2559165.

[3] B. N. Alajmi, I. Abdelsalam, M. I. Marei, and N. A. Ahmed, "A Three-Phase Interleaved AC-DC Converter Based Electric-Vehicle Off-Board Battery Charger Station," *2024 6th International Youth Conference on Radio Electronics, Electrical and Power Engineering (REEPE)*, pp. 1–5, Feb. 2024, doi: 10.1109/reepe60449.2024.10479751.

[4] T. Mamdouh, I. Abdelsalam, and M. I. Marei, "A Three-Phase Totem-Pole AC-DC Converter Based Off-Board Charger for Electric Vehicles," *2025 7th International Youth Conference on Radio Electronics, Electrical and Power Engineering (REEPE)*, pp. 1–6, Apr. 2025, doi: 10.1109/reepe63962.2025.10970995.

[5] K. S. Marcus, I. Abdelsalam, and M. I. Marei, “A Hybrid EV Fast Charging Station,” *2025 7th International Youth Conference on Radio Electronics, Electrical and Power Engineering (REEPE)*, pp. 1–6, Apr. 2025, doi: 10.1109/reepe63962.2025.10971040.

[6] N. Deb, R. Singh, R. R. Brooks, and K. Bai, “A Review of Extremely Fast Charging Stations for Electric Vehicles,” *Energies*, vol. 14, no. 22, p. 7566, Nov. 2021, doi: 10.3390/en14227566.

[7] A. Petrusic and A. Janjic, “Renewable Energy Tracking and Optimization in a Hybrid Electric Vehicle Charging Station,” *Applied Sciences*, vol. 11, no. 1, p. 245, Dec. 2020, doi: 10.3390/app11010245.

[8] H. Arya and M. Das, “Fast Charging Station for Electric Vehicles Based on DC Microgrid,” *IEEE Journal of Emerging and Selected Topics in Industrial Electronics*, vol. 4, no. 4, pp. 1204–1212, Oct. 2023, doi: 10.1109/jestie.2023.3285535.

[9] J. Chen and H. Chen, “Research on the Planning of Electric Vehicle Fast Charging Stations Considering User Selection Preferences,” *Energies*, vol. 16, no. 4, p. 1794, Feb. 2023, doi: 10.3390/en16041794.

[10] A. Al Wahedi and Y. Bicer, “A Case Study in Qatar for Optimal Energy Management of an Autonomous Electric Vehicle Fast Charging Station with Multiple Renewable Energy and Storage Systems,” *Energies*, vol. 13, no. 19, p. 5095, Sept. 2020, doi: 10.3390/en13195095.

[11] G. Arena, A. Chub, M. Lukianov, R. Strzelecki, D. Vinnikov, and G. De Carne, “A Comprehensive Review on DC Fast Charging Stations for Electric Vehicles: Standards, Power Conversion Technologies, Architectures, Energy Management, and Cybersecurity,” *IEEE Open Journal of Power Electronics*, vol. 5, pp. 1573–1611, 2024, doi: 10.1109/ojpel.2024.3466936.

[12] X. Jia, X. Li, T. Yang, D. Hui, and L. Qi, “A Schedule Method of Battery Energy Storage System (BESS) to Track Day-Ahead Photovoltaic Output Power Schedule Based on Short-Term Photovoltaic Power Prediction,” *International Conference on Renewable Power Generation (RPG 2015)*, p. 4 , Jan. 2015, doi: 10.1049/cp.2015.0316.

[13] A. Hussain, Van H. Bui, J.-W. Baek, and H.-M. Kim, “Stationary Energy Storage System for Fast EV Charging Stations: Optimality Analysis and Results Validation,” *Energies*, vol. 13, no. 1, p. 230, Jan. 2020, doi: 10.3390/en13010230.

[14] C. B. Agaton and C. S. Guno, “Renewable energy in sustainable agricultural production: real options approach to solar irrigation investment under uncertainty,” *Renewable Energy and Sustainable Development*, vol. 10, no. 1, pp. 77–91, May 2024, doi: 10.21622/resd.2024.10.1.829.

[15] G. Erdogan and W. Fekih Hassen, “Charging Scheduling of Hybrid Energy Storage Systems for EV Charging Stations,” *Energies*, vol. 16, no. 18, p. 6656, Sept. 2023, doi: 10.3390/en16186656.

[16] M. S. Mastoi *et al.*, “An in-depth analysis of electric vehicle charging station infrastructure, policy implications, and future trends,” *Energy Reports*, vol. 8, no. 2352–4847, pp. 11504–11529, Nov. 2022.

[17] M. M. Mahfouz and M. R. Iravani, “Grid-Integration of Battery-Enabled DC Fast Charging Station for Electric Vehicles,” *IEEE Transactions on Energy Conversion*, vol. 35, no. 1, pp. 375–385, Mar. 2020, doi: 10.1109/tec.2019.2945293.

[18] M. A. H. Rafi and J. Bauman, “A Comprehensive Review of DC Fast Charging Stations with Energy Storage: Architectures, Power Converters, and Analysis,” *IEEE Transactions on Transportation Electrification*, vol. 7, no. 2, pp. 1–1, 2020, doi: 10.1109/tte.2020.3015743.

[19] S. Kumar, I. Ali, and A. S. Siddiqui, “Real time operation of microgrid with variation of distribution generation source to IEEE 13 bus system,” *Renewable Energy and Sustainable Development*, vol. 11, no. 2, p. 424, Nov. 2025, doi: 10.21622/resd.2025.11.2.1572.

[20] P. Das and R. Mitra, “A cyber-physical simulation framework for resilient microgrids with PV, BESS, and tariff-aware control,” *Renewable Energy and Sustainable Development*, vol. 12, no. 1, p. 28, Mar. 2026, doi: 10.21622/resd.2026.12.1.1730.

[21] H. Setiawan, "Towards sustainable energy access: evaluating free online photovoltaic design tools in support of the SDGs," *Renewable Energy and Sustainable Development*, vol. 12, no. 1, p. 41, Mar. 2026, doi: 10.21622/resd.2026.12.1.1757.

[22] M. Eldoromi, A. A. M. Birjandi, and N. M. Dehkordi, "Anti-windup control strategy for interlinking converters in hybrid AC/DC microgrids with EV charging stations," *Electric Power Systems Research*, vol. 247, p. 111800, Oct. 2025, doi: 10.1016/j.epsr.2025.111800.

[23] A. M. Mohammed, S. N. H. Alalwan, A. Taşcıkaraoğlu, and J. P. S. Catalão, "Sliding mode-based control of an electric vehicle fast charging station in a DC microgrid," *Sustainable Energy, Grids and Networks*, vol. 32, p. 100820, Dec. 2022, doi: 10.1016/j.segan.2022.100820.

[24] M. Dicorato, G. Forte, F. Marasciuolo, M. C. Cavarretta, and D. De Michino, "Integration of EV Fast Charging Station into a DC-Based Microgrid," *IEEE Transactions on Industry Applications*, vol. 61, no. 4, pp. 5560–5570, July 2025, doi: 10.1109/tia.2025.3544567.

[25] N. M. Diab, I. Abdelsalam, and M. S. Hamad, "OFF-Board EV Charger Based on Interleaved AC-DC Boost Converter," *2024 International Telecommunications Conference (ITC-Egypt)*, pp. 338–342, July 2024, doi: 10.1109/itc-egypt61547.2024.10620521.

[26] G. Arena, P. Emiliani, A. Chub, D. Vinnikov, and G. De Carne, "DC Fast Charging of Electric Vehicles: a Review on Architecture and Power Conversion Technology," *2023 IEEE 17th International Conference on Compatibility, Power Electronics and Power Engineering (CPE-POWERENG)*, pp. 1–6, June 2023, doi: 10.1109/cpe-powereng58103.2023.10227492.

[27] Z. Zhang, H. Xu, L. Shi, D. Li, and Y. Han, "A unit power factor DC fast charger for electric vehicle charging station," *Proceedings of The 7th International Power Electronics and Motion Control Conference*, pp. 411–415, June 2012, doi: 10.1109/ipemc.2012.6258896.

[28] L. Tan, B. Wu, V. Yaramasu, S. Rivera, and X. Guo, "Effective Voltage Balance Control for Bipolar-DC-Bus-Fed EV Charging Station With Three-Level DC–DC Fast Charger," IEEE Transactions on Industrial Electronics, vol. 63, no. 7, pp. 4031–4041, July 2016, doi: 10.1109/tie.2016.2539248.

[29] H. T. Nguyen *et al.*, "Precise Voltage Regulation of Unbalanced Bipolar DC-Grid-Based Charging Stations: A New Multiobjective Predictive Control Approach," *IEEE Transactions on Power Electronics*, vol. 38, no. 5, pp. 5858–5874, May 2023, doi: 10.1109/tpel.2023.3238054.

[30] A. Choudhury, P. Pillay, M. Amar, and S. S. Williamson, "Performance comparison study of two and three-level inverter for electric vehicle application," *2014 IEEE Transportation Electrification Conference and Expo (ITEC)*, pp. 1–6, June 2014, doi: 10.1109/itec.2014.6861852.

[31] A. Saadaoui, M. Ouassaid, and M. Maaroufi, "Backstepping-Based Control of Vienna Rectifier for Electric Vehicle DC Ultra-Fast Charger," *2022 IEEE 21st Mediterranean Electrotechnical Conference (MELECON)*, pp. 360–365, June 2022, doi: 10.1109/melecon53508.2022.9842893.

[32] W. Ding, C. Zhang, F. Gao, B. Duan, and H. Qiu, "A Zero-Sequence Component Injection Modulation Method With Compensation for Current Harmonic Mitigation of a Vienna Rectifier," *IEEE Transactions on Power Electronics*, vol. 34, no. 1, pp. 801–814, Jan. 2019, doi: 10.1109/tpel.2018.2812810.

[33] M. Schweizer and J. W. Kolar, "Design and Implementation of a Highly Efficient Three-Level T-Type Converter for Low-Voltage Applications," *IEEE Transactions on Power Electronics*, vol. 28, no. 2, pp. 899–907, Feb. 2013, doi: 10.1109/tpel.2012.2203151.

Volume 12, Issue 2, December 2026, e-ISSN 2356-8569
http://dx.doi.org/10.21622/RESD.2026.12.2.1992

[34] B. N. Alajmi, M. I. Marei, I. Abdelsalam, and N. A. Ahmed, "Multiphase Interleaved Converter Based on Cascaded Non-Inverting Buck-Boost Converter," *IEEE Access*, vol. 10, pp. 42497–42506, 2022, doi: 10.1109/access.2022.3168389.

[35] B. N. Alajmi, I. Abdelsalam, M. I. Marei, and N. A. Ahmed, "A Three-Phase Interleaved AC-DC Converter Based Off-Board Battery Charger Station With Balanced Supply and Submodules Currents," *IEEE Transactions on Industry Applications*, vol. 62, no. 2, pp. 2937–2947, Mar. 2026, doi: 10.1109/tia.2025.3618230.